Sedimentation of a suspension of paramagnetic particles in an external magnetic field

J. VESSAIRE, N. PLIHON, R. VOLK, M. BOURGOIN

Univ Lyon, Ens de Lyon, Univ Claude Bernard, CNRS, Laboratoire de Physique, F-69342 Lyon, France

Résumé :

Les écoulements chargés en particules sont omniprésents dans la nature et l'industrie. Souvent l'écoulement est turbulent, les interactions entre les particules et l'écoulement sont complexes de part la nature multi-échelle des structures de la turbulence et les diverses caractéristiques des particules. Dans un systéme réel, il est généralement difficile de démêler les effets spécifiques de ces processus, notamment les effets de couplage pour des particules de tailles finies (interaction particule-particule et particule-écoulement). Le travail, que nous présentons, propose une étude expérimentale du rôle des interactions inter-particulaires : la sédimentation de particules paramagnétiques soumises á la gravité et á un champ magnétique externe dans un fluide initialement au repos. Nos mesures montrent un ralentissement de la décompaction á mesure que le champ augmente, suggérant un possible effet cohésif résultant de la formation de chaînes de forces.

Abstract :

Flows transporting particles are ubiquitous in natural and industrial processes. In most of these situations the carrier flow is turbulent, and the coupling between the particle dynamics and the flow is further complexified by the random and multi-scale nature of turbulence and by the inertia of the particles. However the complexity revealed by previous studies, motivated to consider several simpler situations, trying to separate different physical mechanisms coupling the dynamics of a particle and a flow. Therefore, we propose here to investigate the sedimentation of paramagnetic particles subjected both to gravity and to an external magnetic field, in a initially quiescent fluid. The first observations show a slow down of the decompaction as the magnetic field increases. This observation is compatible with an enhencement of the cohesion of the initial suspension due to magnetic induced dipole-induce dipole interactions generating chain forces.

Key words : Particles-interactions, magnetics particles, sedimentation

Introduction

Flows transporting particles are of interest for fundamental scientific issues, industrial applications and natural systems. In nature, one can mention the formation of rain droplets in clouds, pyroclastic flows, dispersion of pollutants in the atmosphere or planet formation in accretion disks. Regarding industrial

applications, spray combustion in Diesel engines, pneumatic transport of granular media or mixing process are just a few examples. In most of these situations the carrier flow is turbulent, and the coupling between the particle dynamics and the flow is further complexified by the random and multi-scale nature of turbulence and by the inertia of the particles.

When it comes to particles-flow modeling, several situations must be distinguished depending on the nature of the particle. For sufficiently small particles for which a pointwise approximation is relevant, the dynamics is well captured by the celebrated Maxey-Riley-Gatignol equation [7]. Depending on the size and the particle density, corrections to this equation (such as Faxén corrections) can be introduced to some extent. In the recent years, with the democratization of new technologies (high speed cameras, storage and analysis of huge datasets, etc), the experimental study of turbulent transport has revolutionized our capacities to finally charecterize the motion of particles, even in highly turbulent flows [12, 4]. Similar advances have also been achieved in numerical simulations, with the emergence of direct numerical simulations capable to resolve the full dynamics of the particles from first principles [13]. Many of these experimental and numerical studies (see [9, 8, 16, 14] among others) have revealed that is lacking a relevant theoretical framework to model the dynamics of finite size particles, and that improving the usual models (or finding new modeling approaches) is essential to account for subtle effects such as particle-particle interactions, wake effects on particle-flow interaction, disentangling between the effects of inertia and gravity, interplay between clustering, settling and turbulent dynamics, etc.. .

To improve the understanding of such numerous complex coupling effects, it is wise to go step by step and consider first simpler situations in order to disentangle possible individual contributions of different effects. In the present article, we focus on some aspects of the role played by particle-particle interactions, considering the simplified situations where the flow is initially at rest. To this end, we investigate the sedimentation of paramagnetic particle suspension subjected to gravity and a tunable external homogeneous magnetic field in a Hele-Shaw cell (see Fig. 1). In this situation, interaction between particles is tuned by the magnetic field amplitude, while the particles start to settle, a wake develops, which eventually induces further hydrodynamics interactions between particles.

The system under investigation shares features with granular media physics. Over the last decades, numerous studies have indeed investigated the sedimentation of granular suspensions in newtonian fluid [1, 2, 3]. In this context, more recent studies also addressed the question of the nature and the dynamics of interface instabilities in the early stage of sedimentation. In particular, the emergence of a fingering instability has been demonstrated, recalling the well-known Rayleigh-Taylor instability which classically develops at a horizontal interface between two fluids with different densities (the denser being on top) [10, 11]. Several authors have investigated theoretically and experimentally the fingering instability at a particle / fluid interface in a Hele-Shaw cell [6, 17, 15], proposing a purely fluid interpretation *à la* Rayleigh-Taylor.

We propose here to explore the sedimentation of paramagnetic particles subjected both to gravity and to an external magnetic field in fluid at rest, with the goal to broaden the understanding of tunable particle-particle interaction in the sedimentation process. After a brief description of the overall sedimentation process and of the role of magnetization on particle-particle interactions (Section 1), we detail the experimental setup and protocol (Section 2) before presenting the results, focusing on the impact of the magnetic field (and hence on particle-particle interactions) on the initial decompaction of the sediment pack (Section 3). We conclude with a brief discussion of the observed trends and possible future studies.

1 Sedimention of paramagnetic particles with an applied external magnetic field

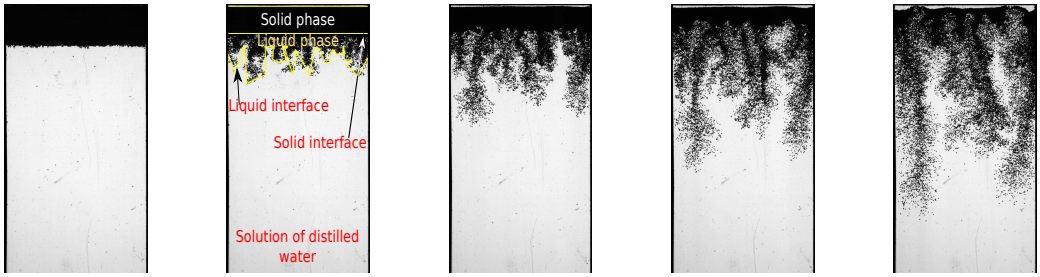

(a) t = 0s (b) t = 1s (c) t = 2s (d) t = 3s (e) t = 4s

FIGURE 1 – *Temporal series of images showing sedimentation subjected to gravity and an horizontal magnetic field in a steady flow with 250µm in diameter paramagnetic particles in a closed Hele-Shaw cell. The cell is 200 mm high, 50 mm wide and 1 mm depth.*

Fig. 1 presents a temporal series of the sedimentation of the paramagnetic particles suspension. The time origin ($t = 0$ s) is defined when the cell reaches the vertical position, after being rotated (see experimental protocol in next section). On the first frame, we see the initial pack of particles, standing above water. The shape of the interface particles-solution is nearly flat. On the next three frames, two main regions can be defined for the particle suspension : (i) in the upper part, particles form a homogeneous and compact pack, at rest, (ii) below the interface is disturbed giving rise to fingers of dispersed sedimenting particles (reminiscent of the Rayleigh-Taylor instability previously mentionned). Following classical granular *jargon* [5], we shall call *solid* phase the upper compact region of particles and *liquid* phase the lower sedimenting region. We therefore distinguish two interfaces : (i) the first between the *solid* and *liquid* phases of particles, (ii) the second between the *liquid* phase of particles and water. As the sedimentation process goes on, the volume of the solid phase reduces (we shall refer to this as the *decompaction* or the *liquefaction* of the solid phase) and at the same time the area of the liquid interface increases (the solid-liquid interface slowly moves up while the liquid-water interface develops larger fingers). In the last frame in Fig. 1, the solid phase has disappeared and the dynamics of the suspension is strongly influenced by the induced recirculation flow of water in the cell. The subsequent behavior of the suspension then becomes strongly affected by confinement effects due to the finite size of the cell.

In the present work we focus on the dynamics of the initial decompaction process of the particle pack (about $t < 4$ s), and investigate the liquefaction rate of the solid phase as well as the growth rate of the liquid phase, with the goal to highlight the impact of particle-particle interactions on the global sedimentation behavior, when imposing a tunable homogeneous magnetic field.

In absence of any external magnetic field ($B_0 = 0$ G), particles are only subjected to gravity $\vec{g}$ (and eventually hydrodynamic interactions).
In presence of magnetic field ($B_0 \neq 0$ G), all particles acquire an induced magnetic moment M given by :

$$\vec{M} = \frac{4}{3}\pi r^3 \frac{\chi_m}{\mu_0}\vec{B}_0 \tag{1}$$

where r is the radius of the particles, μ_0 the vacuum permitivity and χ_m the magnetic susceptibility of the particles. In addition to gravity, each particle is then subjected to the magnetic force exerted by the

magnetization of the other particles. The magnetic force $\vec{f_m^i}$ acting on particle i can then be written as

$$\vec{f_m^i} = -\nabla(\vec{M_i}.\vec{B}) \tag{2}$$

where $\vec{M_i}$ is the induced magnetization of particle i and $\vec{B} = \vec{B_0} + \sum_{k\neq i}^{N_p} \vec{b}_{ki}$ the total magnetic field at the position of particle i, including the applied field $\vec{B_0}$ and the total induced magnetic field $\vec{b_i} = \sum_{k\neq i}^{N_p} \vec{b}_{ki}$ from all other particles than i. Note that as we consider here the case of a homogeneous applied magnetic field $\vec{B_0}$, there is no net force exerted by $\vec{B_0}$ on the magnetized particles and f_m^i is simply given by

$$\vec{f_m^i} = -\vec{M_i}.\nabla(\vec{b_i}) \tag{3}$$

We also recall that the dipolar magnetic field $\vec{b}_{ki}$ generated by a particle k with magnetization $\vec{M_k}$ at the position of particle i is given by

$$\vec{b}_{ki} = \frac{\mu_0}{4\pi}\left(\frac{3\vec{r}_{ki}\left(\vec{M_k}\cdot\vec{r}_{ki}\right)}{|\vec{r}_{ki}|^5} - \frac{\vec{M_k}}{|\vec{r}_{ki}|}\right) \tag{4}$$

where $\vec{r}_{ki}$ is the separation vector between particle k and particle i. Considering the rapid decay of $\vec{b}_{ki}$ with $|\vec{r}_{ki}|$ contributions to $\vec{b_i}$ mostly come from the nearest neighbors, which in the initially compact pack are at a distance $\vec{r}_{ki}$ commensurate with the particle diameter $d = 2r$ (although the orientation of the force may change depending on the position of the considered neighbors around particle i). As a consequence, the typical expected order of magnitude for $\left|\vec{b_i}\right|$ is given by $\mu_0 M/4\pi r^3$, and considering Eqs. 1 & 3, the typical order of magnitude of the magnetic force is

$$\mathcal{O}\left(\left|\vec{f_m^i}\right|\right) \propto \frac{r^2\chi_m^2 B_0^2}{\mu_0} \tag{5}$$

Based on these estimates, we can then define a dimensionless number Ψ comparing the amplitude of magnetic forces and gravity (including effect of buoyancy) acting on each particle :

$$\Psi = \frac{\chi_m^2 B_0^2}{\mu_0 r\left|\rho_p - \rho_w\right| g} \tag{6}$$

with ρ_p and ρ_w the density of the particles and of water respectively. Beyond the expected trends that the role of the magnetic forces should naturally increase with the amplitude of the applied field and the particles susceptibility, this relation interestingly shows that it should also be more pronounced for smaller particles.

2 Experimental Setup

Experiments were performed in a sealed Hele-Shaw cell (200 mm in height, 50 mm in width, with a gap of 1 mm), filled with distilled water and paramagnetic particles. A small amount of surfactant (Sodium dodecyl sulfate) is also added to stabilize the solution and to prevent aggregation of the particles. Fig.-2 shows a schematic of the cell and a typical recorded image of settling particles. The gap of Hele-Shaw cell is fixed by a thin (1 mm in thickness) internal plastic frame clamped between the two plexiglass plates. Two pivots screwed on the sides of the cell at mid-height allow to rotate the cell.

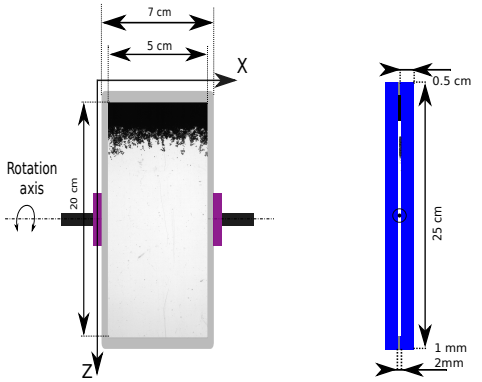

(a) Front view (b) Side view

FIGURE 2 – *Settings of the Hele-Shaw cell.*

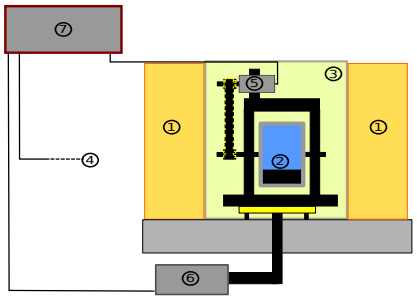

FIGURE 3 – *Experimental setup : 1-coils, 2-Hele-Shaw cell, 3-LED panel, 4-High speed Camera, 5-stepper motor, 6-vibrator pot, 7-Raspberry-Pi.*

The particles are polythene (PE) micro-spheres, with density $\rho_p = 1.2$ g.cm^{-3} doped with iron oxyde (FeO) in order to be paramagnetic (from *BKPMS, Cospheric LLC, Santa Barbara, CA USA*). We had at hands three sets of particles with diameter $d = 250$ μm, $d = 600$ μm and $d = 1000$ μm. Considering the size dependence of the paramter Ψ (Eq. 6) we have chosen to use the smallest particles ($d = 250$ μm) in order to maximize the relative amplitude of inter-particle magnetic forces compared to gravity.
Two coils in Helmholtz configuration surround the cell in order to apply a homogeneous magnetic field $\vec{B}_0$, parallel to the x axis, aligned with the width of the cell (Fig. 3). The coils are driven with a 10 kW power supply (*Danfysik System 9100*). When fed by the maximum available current, a rapid increase of the coils temperature is observed, requiring an efficient coil cooling from dedicated recirculation of cold water. The maximum amplitude of the applied magnetic field is $B_0^{max} \approx 0.12$ T.
In order to carry a systematic investigation with good statistical convergence, for a given value of the applied magnetic field, numerous (typically 100) sedimentation experiments are repeated by successively rotating the cell. For a good reproducibility of experimental conditions, the setup is fully automatized, the rotation been ensured by a stepper motor controlled from a Raspberry Pi nano-computer with a pre-programmed cycle. Special care has been taken to properly condition the pack of particles in between rotations in order to have an initial interface as flat and horizontal as possible. This is achieved imposing several rapid partial rotations and simultaneously vibrating the cell with an electrodynamics shaker. Our optimal pack conditioning protocol is also automatized and is part of the global rotation cycle controlled by the nano-computer.

Measurements are then based on high-speed backlight imaging of the cell, wich is illuminated from behind by a LED panel. Recordings are performed using a high speed camera (*Flare 2M360-CL, IO Industries*) running with a resolution of 2048x1088 pixels at a frame rate of 300 fps. The starting of the recordings is triggered by the controller nano-computer in synchronization with the rotation cycle.

In this cycle, each rotation therefore consists on several successive steps :

1. The pack is packed in a flat horizontal interface.
2. The cell is rapidly rotated with a controlled rotation speed of 200 rpm (half a rotation to bring the pack up is therefore achieved in 150 ms).
3. The recording starts when the cell attains its vertical position (a few pre-triggered frames are recorded to better detect, after post-processing, the time origin when the cell so that reaches its vertical position).

As already mentioned, all devices are controlled by a nano-computer. The sequence of experimental cycle can be repeated as many times as desired. This ensures an optimum reproducibility of experimental conditions and allows good statistical convergence.

3 Experimental Results

We present in this section results on the *liquefaction* rate of the *solid* phase and the simultaneous growth of the *liquid* phase of the suspension in the early stage of the sedimentation, right after the cell reaches its vertical position. To quantitatively address these questions we use image processing tools to detect the *solid-liquid* and *liquid-water* interfaces.

3.1 Edge detection & area calculation

The successive image processing steps are illustrated in Fig. 4 (note that, compared to previous figures, negative images are shown and now particles appear bright).

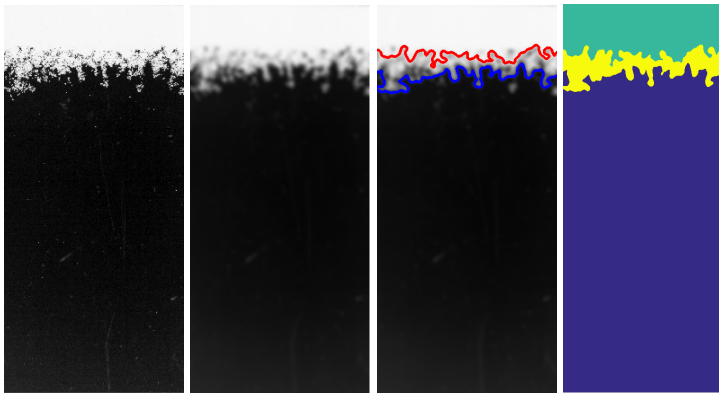

(a) Raw image (b) Fuzzy image (c) Egdes (d) Binarize

FIGURE 4 – *Process of the edges and the areas detection from the raw image.*

Fig. 4(a) shows a raw image, where the *solid* phase appears as a continuous bright region whereas the liquid phase is characterized by some fragmentation of the intensity pattern. We first apply a Gaussian filter in order to blur the image in the liquid phase : as a result (i) nearby particles in the fragmented region become connected and (ii) the locally smoothed intensity in the *liquid* region decreases as shown in Fig. 4(b). We use a Gaussian convolution kernel with a width of 1.5 particle diameter in order to reconnect the fragmented areas up to this scale. Few blobs of particles separated by more than 1.5 d can be present ; those will be considered as having already left the *liquid* phase and are excluded from the detection. Note that the Gaussian filtering has no major effect on the *solid* phase region of the image which has constant and homogeneous intensity. Then, two successive thresholding of the image are operated. The first uses a relatively low threshold chosen in order to keep all the particles (non-dark pixels) in both the *solid* and *liquid* phases. An edge detection algorithm is then run on the binarized image to get the *liquid-water interface* (blue line in Fig. 4(c)). The second thresholding uses a higher value of the threshold, chosen to keep only the bright pixels in the continuous region corresponding to the *solid* phase. Another edge detection then retrieves the *solid-liquid* interface (solid black line in Fig. 4(c)). The different binarized images can also be combined to create a ternary image showing the

solid phase (green region in Fig. 4(d)), the *liquid* phase (yellow region in Fig. 4(d)) and water (blue region Fig. 4(d)).

This image processing sequence is performed for all frames in each recording. In order to monitor the time evolution of the area of both *solid* phase $A_s(t)$ and *liquid* phase $A_l(t)$.
In the sequel, for a given experiment (*i.e.* a given value of the applied magnetic field) we will consider the time evolution of the *solid* and *liquid* phase areas averaged over the ensemble of recordings :

$$\langle A_{s,l}(t)\rangle_{movie} = \frac{1}{N_{movie}} \sum_{k=1}^{N_{movie}} A^k_{s,l}(t), \tag{7}$$

with N_{movie} the number of repeated movie for each experiment ($N_{movie} \approx 100$ in the present study) and $A^k_{s,l}(t)$ the *solid* or *liquid* area estimated at time t from the k^{th} movie. For the sake of clarity, we shall omit from now the average brackets when presenting the results.

3.2 Liquefaction dynamics and particle concentration

3.2.1 Evolution of *solid* and *liquid* phases

Fig. 5(a) shows the time evolution of the *solid* phase area $A_s(t)$ for three different amplitudes of the applied magnetic field ($B_0 = 0 - 320 - 800$ G). After a short period with almost no apparent evolution, we observe a rapid decrease of $A_s(t)$ followed by a slower linear decrease. A first visible impact of the magnetic field appears in the long term behavior, where we see that the *solid* phase *liquefies* slower as the magnetic field increases. At $t = 4$ s we observe indeed that the remaining area of *solid* phase is the largest for $B_0 = 800$ G and the smallest when no magnetic field is applied.

The influence of the magnetic field on the *liquefaction* rate is better apprehended from the *liquefaction velocity* :

$$V_s(t) = -\frac{dA_s(t)}{dt}. \tag{8}$$

(Note that V_s has units of $\mathrm{m^2 s^{-1}}$). Fig. 5(b) shows the time evolution of the *liquefaction velocity*. Two regimes are clearly visible : after a short transient with a rapid increase of the velocity followed by a local maximum, the velocity reaches a constant asymptotic terminal value V_s^∞ . It can be noted that in spite of the large number of recorded movies for each experiment, while the raw curves for $A_s(t)$ appear relatively smooth and well converged, their derivative still exhibit some visible noise in particular in the long term regime. We therefore estimate V_s^∞ by averaging $V_s(t)$ typically on the time interval $t \in [2\text{ s} - 4\text{ s}]$. Equivalently, we could have estimated the terminal velocity from a linear fit of the long term trend of $A_s(t)$.

During the initial transient phase we can notice the presence of the small peak at very short time (around $t \approx 150$ ms), reminiscent of a short damped oscillation of the cell when it stops in the final vertical position. In the subsequent growth of the *liquefaction* velocity a systematic trend can be observed : the larger the magnetic field, the larger the *liquefaction* rate. The mild overshoot preceding the terminal regime occurs at a similar time $t \approx 0.7$ s regardless of the amplitude of the magnetic field.

Concerning the terminal *liquefaction* regime, Fig. 6(a) shows the *liquefaction* average terminal velocity V_s^∞ as a function of the applied magnetic field amplitude. In agreement with the qualitative observed

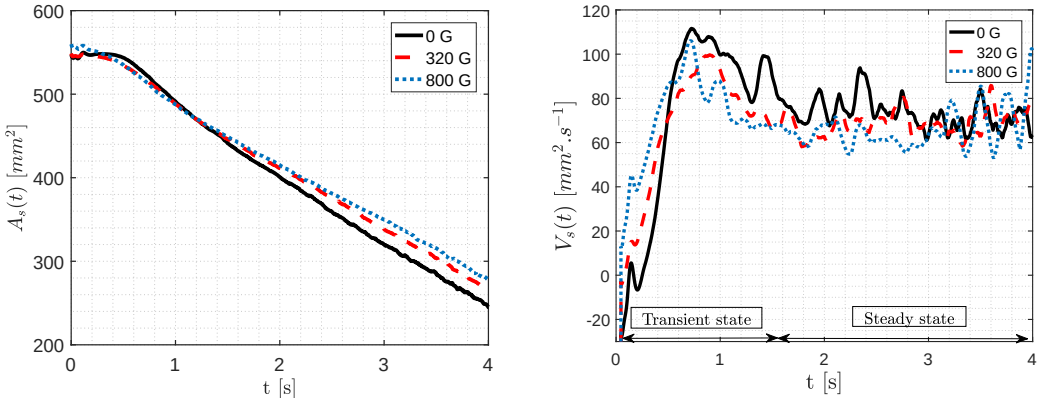

(a) Mean area versus time (b) Mean velocity versus time

FIGURE 5 – *(a) Time evolution of the solid area for different applied magnetic field amplitudes. (b) Time evolution of the erosion velocity. – gravity only :* $B_0 = 0\ G$*;* - - $B_0 = 320\ G$*;* .. $B_0 = 800G$*.*

trend of $A_s(t)$, we see that the terminal *liquefaction* velocity decreases when the magnetic field increases.

A similar analysis has been performed for the growth of the *liquid* phase, defining the *liquid* growth velocity as :

$$V_l(t) = \frac{dA_l(t)}{dt}. \tag{9}$$

Fig. 6(b) shows the *liquid* average terminal velocity as a function of the applied magnetic field amplitude. Trends similar to those of the *liquefaction* velocity are observed : a decrease of the *liquid* growth velocity as the magnetic field increases.

The observed trends for the *solid* and the *liquid* phases are *a priori* consistent : as the magnetic field amplitude increases, the *solid* phase is stabilized (it *liquefies* slower) so that the *liquid* phase is less supplied with particles and hence grows slower. In this scenario, an interesting question in this process concerns the evolution of the particle concentration in the *liquid* phase. The particle concentration results from the balance of the particle supply from the *liquefaction* of the *solid* phase and of the evolution of the *liquid* area $A_l(t)$ (which grows in time). This issue is investigated in the next sub-section.

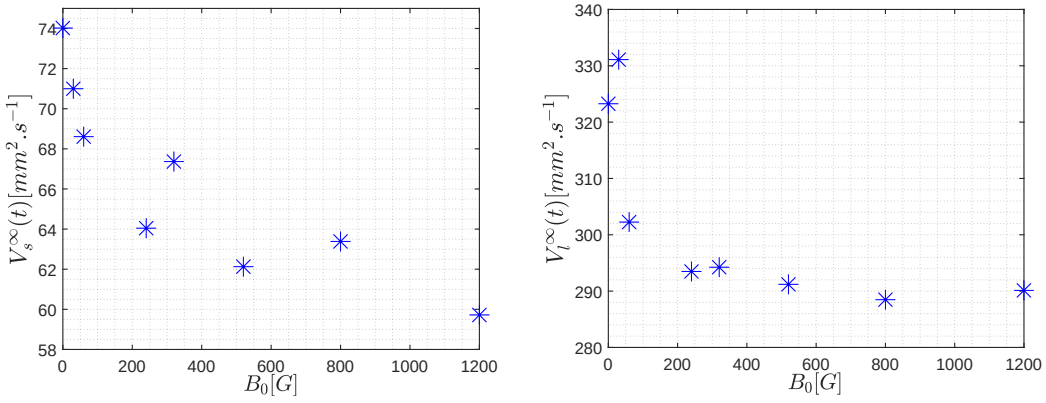

FIGURE 6 – *(a)-Terminal* liquefaction *velocity versus the amplitude of the applied magnetic field, (b)-Terminal velocity for the growth of the* liquid *phase versus the amplitude of the applied magnetic field. Both velocities decrease when the magnetic field increases.*

3.2.2 Particle concentrations in the *solid* and *liquid* phases

The particle concentration ρ_s in the *solid* phase is assumed to be constant and fixed by the compacity of the initial pack. Initially, the *liquid* is empty and emerges when the *solid* phase starts *liquefying*. The particle concentration in the *liquid* phase is therefore expected to have a non-trivial time evolution.

Keeping in mind that the cell is sealed, and hence the total number N_p of remains constant, the density in both phases can be directly related to V_s and V_l. Assuming that all particles remain in the *liquid* and *solid* phases (this approximation neglects the few particle blobs eventually detaching from the *liquid* phase) and that the concentration within each phase is relatively homogeneous, we can indeed write

$$N_p = \rho_l(t)A_l(t) + \rho_s(t)A_s(t). \tag{10}$$

The conservation of the total number of particles then imposes $\mathrm{d}N_p/\mathrm{d}t = 0$ which, considering Eq. 10 and assuming that ρ_s remains constant, leads to

$$\frac{V_s(t)}{V_l(t)} = \Gamma_{ls}(t) + \frac{d\Gamma_{ls}(t)}{dt}\frac{A_l(t)}{V_l(t)}, \quad \text{with} \quad \Gamma_{ls}(t) = \frac{\rho_l(t)}{\rho_s(t)}. \tag{11}$$

This relation directly links the *liquid* to *solid* concentration ratio to the corresponding areas and velocities and in particular to the *solid* to *liquid* velocity ratio $V_s(t)/V_l(t)$, represented in Fig. 7(a). In principle, Eq. 11 is a simple differential equation for Γ_{ls} with empirically known coefficients ($V_s(t)/V_l(t)$ and $A_l(t)/V_l(t)$ are directly accessible from the measurements in the previous section), from which we can derive the time evolution of Γ_{ls}. We will focus here on the long term asymptotic behavior, where the ratio $V_s(t)/V_l(t)$ is constant, and of the order of $V_s^\infty/V_f^\infty \approx 0.25$. In this stationary regime, the solution of Eq. 11 is $\Gamma_{ls} = V_s^\infty/V_f^\infty \approx 0.25$. So that, the *liquid* phase is four times more dilute than the *solid* phase, and the concentration does not depend on the amplitude of the magnetic field.

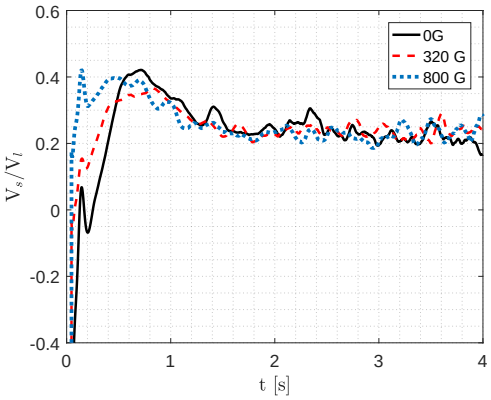

FIGURE 7 – *Time evolution of the* solid *to* liquid *velocity ratio. At the steady state, the* solid *to* liquid *velocity ratio reaches an asymptotic value 0.25, independent of the magnetic field amplitude*

4 Discussion and Conclusion

Overall the influence of an increasing magnetic field on the decompaction of the *solid* pack exhibit several interesting features :

— In the initial phase, the *liquefaction* is accelerated with the magnetic field.
— The terminal *liquefaction* velocity is on the contrary reduced by the magnetic field and so is the growth rate of the *liquid* phase.
— The terminal concentration of the *liquid* phase does not depend on the magnetic field.

Some features of these trends can be quantitatively interpreted in terms of a magnetically induced interaction between the particles. The reduction of the terminal *liquefaction* velocity with magnetic field suggests a stabilizing effect of the magnetic field. A possible interpretation of this could be the formation of chain-forces of particles. The *solid-liquid* interface, structured along magnetic field lines, reinforcing the cohesion of the *solid* phase. The origin of the initial acceleration of the decompaction is less clear. It can result from the vertical repulsion between parallel dipoles from successive layers in the initially compact *solid* phase which could promote the initial destabilization of the interface. Thus loosen, particles in the interface could then self-organize to form the stabilizing chain-forces aforementioned. Finally, the independence of particles concentration in the *liquid* phase, very likely reveals that when the particles are sufficiently dilute (we find the *liquid* phase to be about four times more dilute than the *solid* phase) the typical inter-particle distance is so that the magnetic interaction between induced dipoles becomes negligible compared to gravity and hydrodynamic interaction.In such situation, the magnetic field then is not expected to have any significant impact on the inner structure of the dilute *liquid* phase.

This scenario, which is highly speculative, suggests that most of the action of the magnetic field affects primarily the *solid-liquid* interface. If so, one should expect a clear signature of the magnetic field on the fingering (Rayleigh-Taylor like) instability. The increased particle cohesion scenario by magnetically induced chain-forces can be expected for instance to act as an enhanced surface tension of the interface as the magnetic field amplitude is increased, what has a stabilizing effect. We plan now, in the continuity of this study, to investigate the development of the Rayleigh-Taylor instability, by a systematic investigation of the structure and the dynamics of the *solid-liquid* interface, in order to extract information on the wavelength and growth rate of the instability. We will in particular address the question of the possible interpretation of the role played by the magnetic field in terms of an effective surface tension. Other interesting perspective of this work, will consist in repeating the experiments trying to enhance the influence of the magnetic interactions. Considering the parameter Ψ defined in Eq. 6, this can be done for instance by using smaller particles or ferromagnetic particles (with increased magnetic susceptibility).

Références

[1] R. A. Bagnold. Experiments on a Gravity-Free Dispersion of Large Solid Spheres in a Newtonian Fluid under Shear. *Proc. R. Soc. London*, Ser. A **225**, (1954).

[2] G. K. Batchelor. Sedimentation in a dilute dispersion of spheres. *J. Fluid Mech.*, **52**, (1972).

[3] G. K. Batchelor and R. W. Janse Van Rensburg. Structure formation in bidisperse sedimentation. *J. Fluid Mech.*, **166**, (1986).

[4] M. Bourgoin, J.-F. P., and R. Volk. Lagrangian methods in experimental fluid mechanics. In Thomas von Larcher and Paul D. Williams, editors, *Modeling Atmospheric and Oceanic Flows : Insights from Laboratory Experiments and Numerical Simulations*. (2014).

[5] H. M. Jaeger and S. R. Nagel. Granular solids, liquids, and gases. *Rev. Mod. Phys.*, **68**, (1996).

[6] A. Lange, M. Schröter, M. A. Scherer, A. Engel, and I. Rehberg. Fingering Instability in a Water-Sand Mixture. *Eur. Phys. J. B*, **484**, (1997).

[7] M. R. Maxey and J. J. Riley. Equation of motion for a small rigid sphere in a nonuniform flow. *Phys. Fluids*, **26**, (1983).

[8] N. M. Qureshi, U. Arrieta, C. Baudet, A. Cartellier, Y. Gagne, and M. Bourgoin. Acceleration statistics of inertial particles in turbulent flow. *Eur. Phys. J. B*, **66**, (2008).

[9] N. M. Qureshi, M. Bourgoin, C. Baudet, A. Cartellier, and Y. Gagne. Turbulent transport of material particles : An experimental study of finite size effects. *Phys. Rev. Lett.*, **99**, (2007).

[10] J. W. S. Rayleigh. Investigation of the character of the equilibrium of an incompressible heavy fluid of variable density. *Proc. London Math. Soc.*, **14**, (1883).

[11] G. Taylor. The Instability of Liquid Surfaces when Accelerated in a Direction Perpendicular to their Planes. I. *Proc. R. Soc. London.*, ser. A **201**(1065) :192–196, (1950).

[12] F. Toschi and E. Bodenschatz. Lagrangian Properties of Particles in Turbulence. *Annu. Rev. Fluid Mech.*, **41**, (2009).

[13] M. Uhlmann. An immersed boundary method with direct forcing for the simulation of particulate flows. *J. Comp. Phys.*, **209**, (2005).

[14] M. Uhlmann and A. Chouippe. Clustering and preferential concentration of finite-size particles in forced homogeneous-isotropic turbulence. *J. Fluid Mech.*, **812**, (2017).

[15] J. Vinningland, Ø Johnsen, E. Flekkøy, R. Toussaint, and K. Måløy. Experiments and simulations of a gravitational granular flow instability. *Phys. Rev. E*, **76**, (2007).

[16] R. Volk, E. Calzavarini, G. Verhille, D. Lohse, N. Mordant, J.-F. Pinton, and F. Toschi. Acceleration of heavy and light particles in turbulence : Comparison between experiments and direct numerical simulations. *Physica D*, **237**, (2008).

[17] C. Völtz, W. Pesch, and I. Rehberg. Rayleigh-Taylor instability in a sedimenting suspension. *Phys. Rev. E*, **65**, (2001).